APL Photonics

RESEARCH ARTICLE | MARCH 07 2024

Few-mode metal-free perovskite optical fiber with second-order optical nonlinearity

Hei Chit Leo Tsui ; Dumitru Sirbu ; Naseem Alsaif; Nathan Hill ; Graham Tizzard ; Pablo Docampo ; Noel Healy

APL Photonics 9, 036106 (2024)
https://doi.org/10.1063/5.0186789

Few-mode metal-free perovskite optical fiber with second-order optical nonlinearity

Cite as: APL Photon. 9, 036106 (2024); doi: 10.1063/5.0186789
Submitted: 8 November 2023 • Accepted: 19 February 2024 •
Published Online: 7 March 2024

View Online Export Citation CrossMark

Hei Chit Leo Tsui,[1] Dumitru Sirbu,[1] Naseem Alsaif,[1] Nathan Hill,[1] Graham Tizzard,[2] Pablo Docampo,[3] and Noel Healy[1,a)]

AFFILIATIONS

[1] Emerging Technologies and Materials Group, School of Mathematics, Statistics and Physics, Newcastle University, Newcastle NE1 7RU, United Kingdom
[2] School of Chemistry, University of Southampton, Southampton SO17 1BJ, United Kingdom
[3] School of Chemistry, University of Glasgow, Glasgow G12 8QQ, United Kingdom

[a)] **Author to whom correspondence should be addressed:** noel.healy@newcastle.ac.uk

ABSTRACT

Semiconductor core optical fibers are highly desirable for fiber-based photonic and optoelectronic applications as they can combine strong optical nonlinearities, tight light confinement, wide transmission bands, and electronic functionality within a single platform. Perovskites have emerged as particularly exciting materials for semiconductor photonics as they have strong optical nonlinearities and tunable optoelectronic bandgaps. However, lead-based perovskites contain toxic elements and are, therefore, not environmentally friendly. Furthermore, in fiber form, their core-size is prohibitively large, making them unsuitable for nonlinear optics and applications that require single-mode guidance, such as telecommunications. Here, we report a metal-free perovskite core optical fiber where lead has been substituted for an ammonium cation in the perovskite structure. The core material has a wide bandgap greater than 5 eV, a high laser damage threshold, and a core diameter that can be produced as small as 5 μm. At this core size, the fiber supports just six modes, and the fundamental mode can readily be excited and isolated. Moreover, the metal-free perovskite has a second-order susceptibility that is absent in the archetypal lead-based perovskites and many other semiconductor core materials, such as silicon and germanium. The second-order susceptibility is important for many nonlinear optics applications, such as second-harmonic generation and quantum optics.

I. INTRODUCTION

Semiconductor core optical fibers are a relatively nascent technology that provides excellent nonlinear and electro-optical properties in a waveguide architecture. These properties have been leveraged in a wide range of devices, including photovoltaic cells, in-fiber detectors, all-optical modulators, and supercontinuum generators.[1–8] To date, most of the demonstrators have used simple unary semiconductor core materials such as silicon and germanium, but, more recently, there has been increasing interest in more complex binary and ternary semiconductor systems.[9–14] These have extended the functionality of the platform, for example, by providing direct bandgap materials for efficient light sources or photo-detectors.[10,15–17] While efforts have been made to incorporate perovskite nanocrystals in optical fiber-type applications,[18–20] one exciting development in the field is the demonstration of semiconductor optical fibers with organometallic halide perovskite cores.[21,22] Perovskites have superlative electronic, optical, and nonlinear optical properties, and their integration with the fiber platform represents a step change for functional optical fiber technologies. The highly tunable nature of the material means that its properties can be tailored for specific target applications. For example, the high third-order nonlinearity, efficient light emission, and selectable bandgap could, in the future, be harnessed for applications that generate, convert, guide, and detect light.[23–33]

Aside from the obvious toxicity issues associated with the lead content, there are other shortcomings in the current state-of-the-art of perovskite optical fibers that preclude their use for the above mentioned applications. For example, nonlinear optics require high energy densities, and for a fiber device, this means a small core

or, more specifically, tight confinement of the propagating mode. The current method of producing perovskite optical fibers uses a solution-based, space-confined, inverse temperature crystallization approach, and owing to issues with solvent transport, the smallest core diameter of glass-clad perovskite optical fibers achievable is upward of 100 μm.[22] By using PTFE in place of the glass cladding, modified wetting kinetics allow for further reduction of the core diameter down to 50 μm. At these core sizes, the optical fibers are highly multi-moded and not amenable to nonlinear optics applications. Furthermore, the archetypal perovskites are designed to

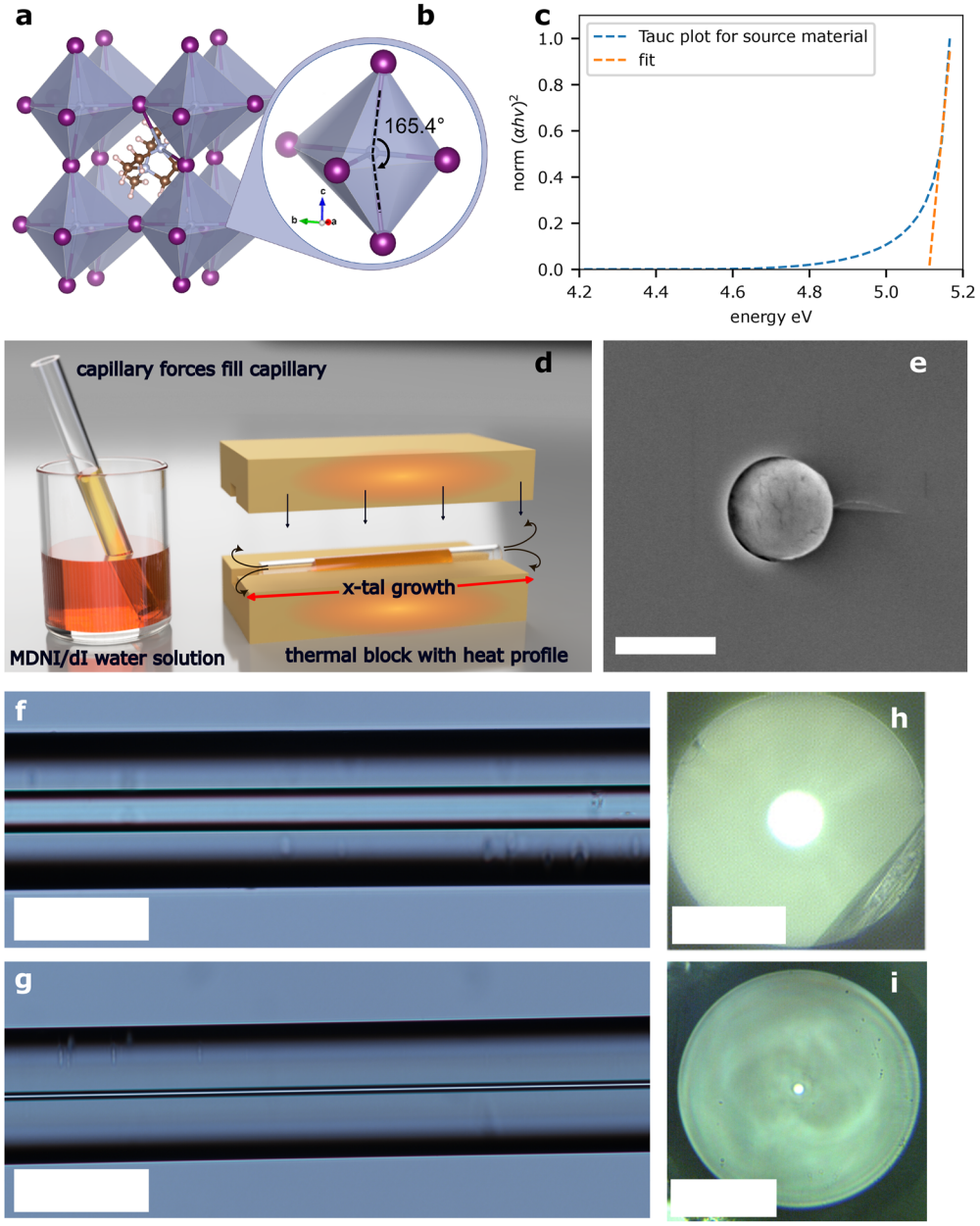

FIG. 1. (a) Side view of the MDNI crystal packing showing the octahedra. (b) Highlight of the distortion of the NH_4I_6 octahedra responsible for the emergence of a non-zero second-order susceptibility. (c) A Tauc plot generated from UV-VIS (Fig. S2) measurements of the synthesized MDNI crystal. (d) Schematic of the capillary action method of precursor solution deposition and subsequent crystallization. (e) Scanning electron microscope image of the cleaved cross section of a 5 μm MDNI core optical fiber, scale bar 5 μm. (f) Diascopic image of the side of a 25 μm MDNI core optical fiber, scale bar 100 μm. (g) Diascopic image of the side of a 5 μm MDNI core optical fiber, scale bar 100 μm. Diascopic illumination and microscope image of (h) a 25 μm MDNI core optical fiber and (i) a 5 μm MDNI core optical fiber, showing white light confined to each core, scale bars 50 μm.

absorb visible light and are, therefore, not attractive for waveguiding in the visible region of the spectrum.

In this work, we explore an iodide-based metal-free perovskite[34,35] as the core material for an optical fiber. Here, we substitute the metal Pb^{2+} center in the hybrid perovskite archetypal structure for an NH_4^+ cation and use methyl-1,4-diazoniumbicyclo[2.2.2]octane ($MDABCO^{2+}$) as the spacer cation, yielding Methyl-DABCO Ammonium Iodide (MDNI).[36]

This immediately addresses the problem of toxicity but also presents other exciting opportunities. We have previously shown that MDNI maintains the strong third-order nonlinearity associated with the perovskite crystal structure, and it has a wide bandgap of greater than 5 eV, making it a strong candidate for nonlinear optics applications from the near-infrared to the ultraviolet.[36] The incorporation of the polar MDBACO cation into the lattice produces a corner-sharing 3D trigonal R_3 perovskite structure with ammonium halide octahedra; Fig. 1(a). As shown in Fig. 1(b), these octahedra are distorted, which means that the crystal is not centrosymmetric, making them ferroelectric materials with a permanent dipole at room temperature and, therefore, a non-zero second-order nonlinearity that, in this instance, is predicted by density functional theory to be 2 pm V^{-1}; moreover, such as the third order nonlinearity, this is highly tunable by varying the spacer cation.[36,37] In fact, previous studies show that ferroelectricity in these materials is responsible for efficient and polarization-dependent second-harmonic generation (SHG).[38] These properties and resulting capabilities, i.e., SHG and parametric down-conversion, coupled with simple processability and high laser damage thresholds, make this emerging family of metal-free perovskites extremely attractive for optoelectronic and quantum optics applications.

Here, we present the first demonstration of an optical fiber with a metal-free perovskite (MDNI) core. By adopting a conventional crystallization process, i.e., controlled cooling, fibers with core sizes of 5 μm can be readily produced within a glass (SiO_2) cladding. The fiber is few-moded and supports just six modes, with the fundamental mode tightly confined to the core, thus providing a route to perovskite fiber-based nonlinear optics. We demonstrate this potential by showing second-harmonic generation in the core, which is permitted by the non-centrosymmetric core material, a property that eludes the organometallic halide perovskite family.

II. RESULTS AND DISCUSSIONS

A. Fabrication of metal-free perovskite optical fibers

Large crystals of MDNI were synthesized using the protocol outlined in the experimental section, and the crystal structure of MDNI was confirmed using x-ray diffraction, see the supplementary material, Fig. S2. Figure 1(c) shows a Tauc plot derived from UV-VIS measurements (Fig. S3, the supplementary material), confirming the expected wide bandgap of the material to be 5.11 eV. The core of the optical fiber is grown from a solution of this source, MDNI, in deionized water. The silica cladding capillaries can be filled with the solution via capillary action, or, for longer lengths, a method of forcing the liquid into the capillary can be used; see Fig. 1(d). The crystalline core material is grown from the solution by placing it in an oven and slowly cooling the liquid from 95 °C to room temperature, i.e., via standard supersaturation, nucleation, and growth; Fig. 1(d). Here, the concentration is higher at the edge of the capillary tube as water is slowly evaporated, nucleating the crystal and promoting its slow growth across the tube. This process negates the solvent transport issues associated with the inverse temperature crystallization approach and allows the growth of the core material at orders of magnitude smaller core dimensions without having to substitute or modify the silica cladding capillaries for alternative, less optical fiber network-compatible materials. A detailed description of the fiber fabrication is provided in the experimental section.

Figure 1(e) shows an SEM of the cross section of a cleaved 5 μm core diameter MDNI optical fiber that has been deposited by this approach. It is clear that the core completely and conformally fills the capillary cladding. Figures 1(f) and 1(g) show diascopically illuminated microscope images of longitudinal sections of (f) a 25 μm core diameter MDNI core optical fiber and (g) a 5 μm MDNI core diameter optical fiber. The core material is highly transparent, owing to the high quality of the crystal and its wide bandgap. The deposited structures can have a uniform cross section for as long as 3 cm, which represents an aspect ratio of 3×10^5 for the 5 μm core optical fiber (Fig. S1, the supplementary material). The end faces of the optical fibers can be readily polished using a standard "dry" optical fiber polishing procedure. Figures 1(h) and 1(i) are microscope images of the polished (h) 25 μm and (i) 5 μm fibers under diascopic illumination, and both clearly show white light being guided by the core. A transmission spectrum from the ultraviolet to the near infrared can be seen in the supplementary material in Fig. S4.

B. Characterization of the core material of metal-free perovskite optical fibers

Raman spectroscopy measurements of the 5 μm MDNI fiber were undertaken by focusing a 532 nm laser through the cladding of the fiber onto the core and collecting the scattered light. This spectrum was compared to that of a single crystal of MDNI taken using the same conditions; both are shown in Fig. 2(a). The low-frequency Raman modes, between 80 and 400 cm^{-1}, can be assigned to the lattice modes, and these have a broad, weak signal in both the single crystal and the MDNI fiber, which can be attributed to the dynamic disorder of the organic ions.[39] The $MDABCO^{2+}$ related vibrations between 600 and 1200 cm^{-1} exhibit strong, sharp peaks, and the comparison between the single crystal and the core material indicates a high degree of core material crystallinity. Lorentzian fitting of the peak at 696 cm^{-1} for each spectrum, shown in Fig. 2(b), indicates that the MDNI fiber core and the single crystal sample have very similar full-width at half-maximum, measured to be 3.11 and 3.1 cm^{-1}, respectively. This result shows that the core material of the fiber is highly crystalline. The symmetry of the peak for the fiber core material is further evidence of the high crystallinity, as asymmetry can be caused by a high concentration of crystalline defects.

X-ray diffraction (XRD) was performed on the grown core material that was ground from the cores of the 25 μm MDNI optical fiber, and the result was compared to that of a powder created from a single crystal of MDNI. These results are shown in Fig. 2(c) and confirm good phase purity in the MDNI core material. To further investigate the crystalline nature of the core material, both MDNI optical fibers were mounted in a Lindemann tube, and single crystal XRD experiments were undertaken along the length at predetermined intervals. The spot-size of the x-ray beam was 85 μm, thus

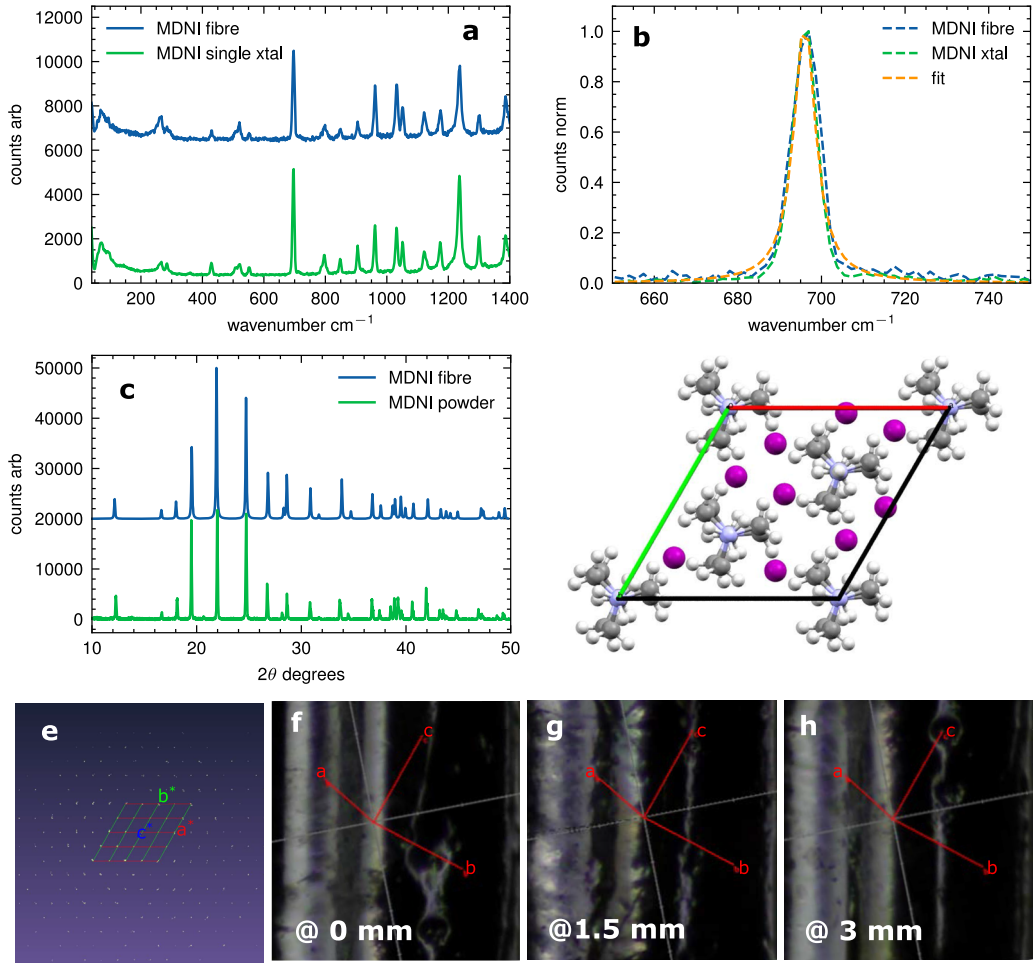

FIG. 2. (a) Raman spectra of the core material (blue) and a single crystal of MDNI (green). (b) Normalized peak of the Raman spectra at 696 cm^{-1} and the Lorentzian fit for the core material. (c) *X*-ray diffractograms of the MDNI core material (blue) and a powdered MDNI sample (green). (d) Single crystal XRD resolved crystal structure of MDNI core material showing the packing of the crystal. Pink = I, white = H, gray = C, and light purple = N. (e) Orthogonal projection of the Ewald sphere along the crystallographic reciprocal *c*-axis of a single crystal measured in the 5 μm core MDNI fiber. Image of 25 μm core fiber hosted in a mounting capillary with an overlay of the measured crystallographic direct axes overlaid at three different positions: (f) 0 mm, (g) 1.5 mm, and (h) 3 mm.

sampling the entire core diameter of each fiber. Although large single crystals are observed in these measurements, they were randomly oriented, and there was no preferential orientation of the crystal within each core, which has been evident in other semiconductor optical fiber crystallization technologies.[40] The crystal structure was resolved to be trigonal in the R_3 space group with a lattice parameter of $a = 9.7018(2)$ Å, $b = 9.7018(2)$ Å, $c = 13.4526(4)$ Å, $\alpha = 90°$, $\beta = 90°$, and $\gamma = 120°$, consistent with that expected for MDNI.[35] Figure 1(d) is an image of the resolved crystal structure demonstrating the R_3 space group packing. Figure S5 of the supplementary material, provides views along the *a*, *b*, and *c* axes. Figure 1(e) shows the Ewald sphere generated via x-ray diffraction of a 5 μm MDNI fiber core, showing a single crystal across the entire core diameter. The estimated average grain size in the 5 μm core fiber was of the order of 100 μm, with the largest length of a single crystal being in the order of 1 mm (Fig. S7, the supplementary material). Figures 1(f)–1(h) show the orientation of the crystal projected onto the 25 μm core fiber as mounted and at the position of measurement. These projections show that there is a dominant crystal along the entire 3 mm sampled region, with some crystal twinning observed (Fig. S7, the supplementary material). The reduction in crystal grain size as related to reduced core sizes led us to use the 5 μm core fiber as the smallest for our optical measurements, as this provided a good balance between material quality and transmitted energy density for nonlinear applications.

C. Perovskite optical fiber characterization

Figures 3(a) and 3(b) show light transmitted through a 1 cm length of 5 μm MDNI core optical fiber at 633 and 1550 nm,

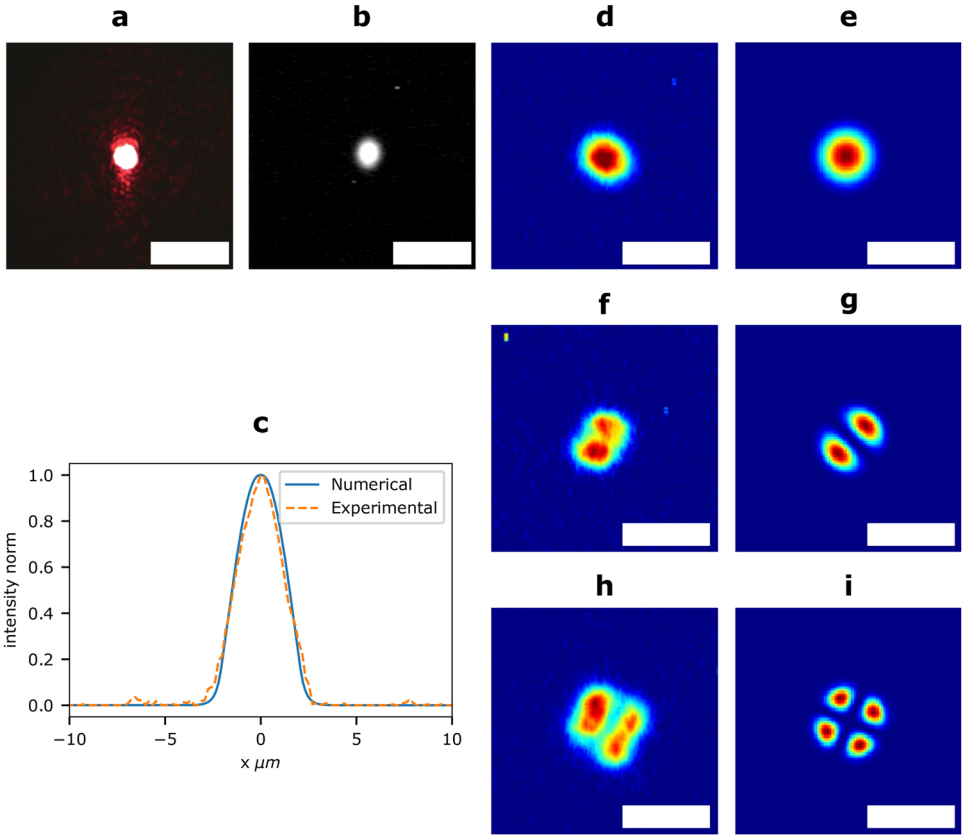

FIG. 3. (a) Transmission of light with a wavelength of 633 nm through a 5 μm MDNI core optical fiber, scale bar 15 μm. (b) Transmission of light with a wavelength of 1550 nm through a 5 μm MDNI core optical fiber, scale bar 15 μm. (c) Measured (orange dashed) and simulated (blue) mode profiles from the 5 μm MDNI core optical fiber transmitting 1550 nm light in the fundamental mode. Intensity profile of 1550 nm light transmitted in the 5 μm MDNI core optical fiber via the LP01 mode (d) (experimental) and (e) (numerical simulation), the LP11 mode (f) (experimental) and (g) (numerical simulation), and the LP21 mode (h) (measured) and (i) (numerical simulation), scale bars 10 μm.

respectively, demonstrating the high bandwidth capability of the optical fiber. The wide bandgap of MDNI would, in principle, guide light with low loss down to 250 nm. A detailed optical characterization of the 5 μm MDNI core optical fiber was undertaken at the important telecommunications wavelength of 1550 nm. The optical transmission loss of the fiber was measured using the standard cut-back approach, and a loss of 3 dB cm^{-1} was determined, which is commensurate with state-of-the-art semiconductor optical fibers. For this experiment, 1 mm sections were removed from a 1 cm length of fiber. At these short lengths, it is important that stray cladding light does not lead to underestimation of the losses; however, as is shown in Figs. 3(b) and 3(c), all of the light is very tightly confined to the small core. We attribute the losses in the fiber to defects and grain boundaries in the crystalline core. A clear route to reducing these losses would be to increase the core's crystallinity via further optimization of the deposition process. The core material of the fiber has a refractive index of $n_1 = 1.58$ at 1550 nm, and the V-number given by $V = \frac{2\pi a}{\lambda}\sqrt{n_1^2 - n_2^2}$ is 6.48, where λ is the operating wavelength, a is the core radius, and the cladding refractive index is $n_2 = 1.444$. As $\Delta n \ll 1$, the low order modes can be considered LP modes, and at $V = 6.48$, the fiber can support six LP modes.

An infrared camera was used to image the near-field modes that could be excited in the fiber. Figures 3(d), 3(f), and 3(h) show the experimentally imaged LP01, LP11, and LP21 modes, which show good agreement with the same modes produced by finite element modeling simulations of the same fiber, shown in Figs. 3(e), 3(g), and 3(i) (see the supplementary material, Fig. S8 for simulation of all modes supported by the fiber). Importantly, the coupling is preferentially obtained in the fundamental LP01 mode, with the higher order modes only being isolated when the input beam is launched off-axis to the core. The slight asymmetries seen in the mode profiles of the higher order modes are most likely due to modest mixing between the allowed modes. Concerning the fundamental mode, the full-width at half-maximum (FWHM) value at the $1/e^2$ power level is 3.8 μm, which matches well with the 3.7 μm predicted by our

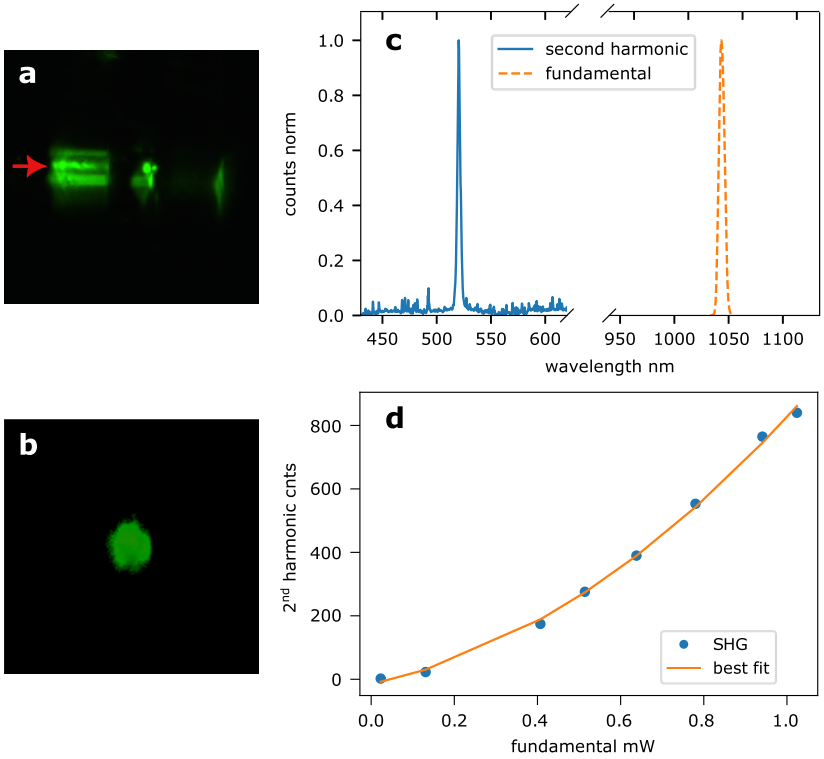

FIG. 4. (a) Image of second-harmonic generated light scattered as it propagates through the 5 μm MDNI core optical fiber (black regions are where the fiber is held to v-groove). (b) The second-harmonic light that is confined to the core as it exits the output of the optical fiber. (c) Spectrum of the fundamental pump beam (orange) and the transmitted second-harmonic (blue) through a 5 μm MDNI core optical fiber. (d) The dependence of the second-harmonic generation on the fundamental pump power shows a parabolic relationship.

model; see Fig. 3(c), and with the 3.74 μm predicted by the Marcuse equation at the fiber's V-number.[41] The effective mode area of fundamental mode for this fiber is 11 μm^2, which is two orders of magnitude smaller than the state-of-the-art polymer-clad perovskite fibers and more than three orders of magnitude smaller than the glass-clad organometallic halide perovskite equivalent. Moreover, being able to excite and isolate the fundamental mode is of particular value for nonlinear optics applications.

D. Second-harmonic generation

To demonstrate the fiber for nonlinear optics applications, we exploit the lack of centrosymmetry in the core material's crystal structure, which gives rise to a second-order susceptibility. A 5 μm diameter core MDNI fiber is set up in a transmission measurement configuration similar to that used to determine the linear optical propagation characteristics. A laser with a wavelength of λ_p = 1040 nm, a pulse duration of 300 fs, and a repetition rate of 1 kHz was coupled into the optical fiber's fundamental mode. The peak power of the pump laser was increased to elicit a nonlinear response from the transmitted light–matter interaction. As the second-harmonic associated with the pump is expected to be at a wavelength of 520 nm, i.e., green, it was relatively straightforward to detect, filter, and image using a CCD camera, as illustrated in Fig. 4(a), which shows the second-harmonic response along the length of the fiber. An image of the second-harmonic light that has been transmitted through the fiber is shown in Fig. 4(b), and in this instance, the second-harmonic output has been coupled to higher-order modes in the fiber. At this wavelength, the fiber has a V = 20 and supports ~200 modes. This offers the prospect of modal phase-matching of the second-harmonic to the pump, but we note here that no attempt at phase matching was undertaken in this work. The transmitted light was coupled into a spectrometer, and the spectra of the pump and second-harmonic are shown in Fig. 4(c). As expected, the central wavelength of the second-harmonic is 520 nm, half that of the fundamental pump. It is also clear that second-harmonic narrowing is present and that the FWHM of the second-harmonic is 0.42× that of the fundamental; this is identical to the narrowing measured for KDP and close to the theoretically predicted $1/2\sqrt{2}$.[42] Figure 4(d) plots the power dependence of the second-harmonic signal, exhibiting a clear quadratic relation, which further confirms that the visible signal is produced by the second-harmonic originating from the core material's second-order nonlinearity.

III. CONCLUSION

We have demonstrated the first optical fiber employing a metal-free perovskite as the core material. We demonstrate that the MDNI crystalline core can be grown via simple cooling of a

supersaturated solution, opening up a route for fiber fabrication with the wide array of metal-free perovskites that are being developed. The fiber that we have presented in this work is a few-mode fiber that allows robust, single-mode operation while maintaining tight light confinement in the active core material. This is an important step for perovskite optical fibers, as single-mode operation is important for many applications, including those in telecommunications. Unlike the archetypal organometallic perovskites that were designed for solar applications, the metal-free MDNI core material has a wide bandgap and permits the guidance of visible light. Furthermore, MDNI, such as many metal-free perovskites, lacks a centrosymmetric crystal structure, which means that it can be used for many important second-order nonlinear optical applications, for example, electrooptic modulation, harmonic generation, and parametric down-conversion.[43] Owing to the versatility of the perovskite structure, these materials can be developed to enhance their nonlinear properties and be able to produce fiber waveguide devices for a wide-ranging set of applications, for example, all-optical signal processing, supercontinuum generation, frequency comb generation, and quantum optics.[44]

IV. EXPERIMENTAL

A. MDNI synthesis

1,4-Diazabicyclo[2.2.2]octane (DABCO), NH_4I, and HI (57% w/w stabilized with 1.5% H_3PO_3) were purchased of the highest purity available and used as received. N-Methyl-1,4-diazabicyclo[2.2.2]octan-1-ium (MDABCO) iodide was synthesized as described elsewhere.[45,46] 0.5 mol of MDABCO iodide and ammonium iodide were dissolved in an aqueous HI solution (20%, stabilized with 0.5% H_3PO_3) at 90 °C. Cooling the pale yellow solution to room temperature resulted in the precipitation of white polycrystalline material. Washing with EtOH and Et_2O and drying in a vacuum gave MDNI a white, crystalline solid with a 70% yield. MDNI monocrystals for Raman spectroscopy were grown by first forming a saturated solution of MDNI in DI water at 90 °C, followed by slow cooling down to 60 °C. Over several days, large monocrystals of MDNI were formed.

B. MDNI fiber production

Capillary tubes were used, as received from polymicro. The tubes were warmed on a hotplate at 95 °C, then dipped in a solution of 0.2 g MDNI powder that was fully dissolved in 0.16 ml of deionized water that had been filtered through a 0.45 μm hydrophilic filter and kept at 95 °C to allow the solution to fill the tube through capillary action. The tubes were then introduced into a homemade "crystallization oven" consisting of two metal plates and a spacer that was pre-warmed to 95 °C. The filled capillary was held in the oven for 24 h at 95 °C to ensure that any crystal that might have formed in the setup phase would redissolve and, second, to start the crystal formation through evaporation at the capillary edge. The fiber was then cooled down slowly at a linear rate of 0.5 °C h^{-1}.

C. Materials characterization

Powder x-ray diffraction data of the produced MDNI were acquired on a Bruker D8 Advance diffractometer in the coupled theta/two theta regime. Single crystal measurements were taken of the MDNI fiber mounted in a Lindemann tube. The data were collected using an Oxford Cryosystems low-temperature device operated at $T = 100(2)$ K and a Rigaku FRE+ equipped with VHF Varimax confocal mirrors, an AFC12 goniometer, and a HyPix 6000 detector diffractometer. The resulting data were resolved using Rigaku CrysAlis Pro. Raman spectra were collected in the backscattering geometry with 0.5 mW, 532 nm laser excitation focused to a spot size of 1 μm using a Horiba Raman microscope.

D. Linear optical characterization

The optical transmission losses of the fibers were measured using the standard cut-back technique. The fiber was mounted in a larger host capillary and polished using standard "dry" fiber polishing methods, i.e., no liquid lubricants were used. A low power continuous wave 1550 nm laser diode was used with an output power of 2 mW. The laser was launched into the core of the fiber using a 0.65 NA anti-reflection coated fused silica objective that was selected to ensure the light was coupled predominantly into the fundamental core mode. The output of the fiber was imaged using an interlaced CCD IR camera to confirm that transmission occurred only through the semiconductor core, thus providing a good indication of the bulk MDNI material quality. The coupling was optimized using a set of Thorlabs Nanomax stages. The measurements were performed on sections of fiber that were 1 cm in length, and each cutback removed ~1 mm of the fiber. Modal isolation was undertaken using off-axis launching of light, and the light was coupled out of the fiber using a 0.65 NA lens that is greater than the fiber's NA. The captured light was imaged using the interlaced CCD IR camera, and coupling into each mode was optimized using the Nanomax stages while observing the imaged output.

E. Nonlinear optical characterization

The 5 μm core MDNI optical fiber was prepared in the same manner as for the linear optical characterization measurements. A spectra physics spirit-one femtosecond laser with a wavelength of 1040 nm, a repetition rate of 1 kHz, and a pulse duration of 300 fs was launched into the fundamental mode of the fiber using a 0.65 NA anti-reflection coated fused silica objective, and the coupling was optimized using Thorlabs Nanomax stages and viewing on a near-IR CCD camera. The second-harmonic output was imaged on a visible CCD camera with an integration of ten frames.

SUPPLEMENTARY MATERIAL

See the supplementary material for additional information.

ACKNOWLEDGMENTS

This work was supported by the UK's Engineering and Physical Sciences Research Council (EPSRC) on Grant No. EP/S031103/1. We thank the EPSRC UK National Crystallography Service at the University of Southampton for the collection of the crystallographic data.

AUTHOR DECLARATIONS

Conflict of Interest

The authors have no conflicts to disclose.

Author Contributions

H. C. L. Tsui: Investigation (lead); Methodology (equal); Resources (equal); Writing – original draft (equal); Writing – review & editing (equal). **D. Sirbu**: Methodology (equal). **N. Alsaif**: Resources (equal). **N. Hill**: Resources (equal). **G. Tizzard**: Investigation (supporting). **P. Docampo**: Funding acquisition (equal); Supervision (supporting). **N. Healy**: Conceptualization (lead); Funding acquisition (lead); Investigation (supporting); Supervision (lead); Writing – original draft (equal); Writing – review & editing (equal).

DATA AVAILABILITY

The data that support the findings of this study are available from the corresponding author upon reasonable request.

REFERENCES

[1] F. A. Martinsen, B. Smeltzer, M. Nord, T. Hawkins, J. Ballato, and U. Gibson, "Silicon-core glass fibres as microwire radial-junction solar cells," Sci. Rep. **4**, 6283 (2014).

[2] R. He, T. D. Day, M. Krishnamurthi, J. R. Sparks, P. J. Sazio, V. Gopalan, and J. V. Badding, "Silicon *p-i-n* junction fibers," Adv. Mater. **25**, 1461–1467 (2013).

[3] R. He, P. J. Sazio, A. C. Peacock, N. Healy, J. R. Sparks, M. Krishnamurthi, V. Gopalan, and J. V. Badding, "Integration of gigahertz-bandwidth semiconductor devices inside microstructured optical fibres," Nat. Photonics **6**, 174–179 (2012).

[4] P. Mehta, N. Healy, T. Day, J. Badding, and A. Peacock, "Ultrafast wavelength conversion via cross-phase modulation in hydrogenated amorphous silicon optical fibers," Opt. Express **20**, 26110–26116 (2012).

[5] T. Sørgård, T. Hawkins, J. Ballato, U. L. Österberg, and U. J. Gibson, "All-optical high-speed modulation of THz transmission through silicon core optical fibers," Opt. Express **29**, 3543–3552 (2021).

[6] L. Shen, N. Healy, L. Xu, H. Cheng, T. Day, J. Price, J. Badding, and A. Peacock, "Four-wave mixing and octave-spanning supercontinuum generation in a small core hydrogenated amorphous silicon fiber pumped in the mid-infrared," Opt. Lett. **39**, 5721–5724 (2014).

[7] A. C. Peacock, J. Ballato, J. Campling, A. F. J. Runge, H. Ren, L. Shen, O. Aktas, P. Horak, N. Healy, and U. J. Gibson, "Wavelength conversion and supercontinuum generation in silicon optical fibers," IEEE J. Sel. Top. Quantum Electron. **24**, 5100309 (2018).

[8] R. Sohanpal, H. Ren, L. Shen, C. Deakin, A. M. Heidt, T. W. Hawkins, J. Ballato, U. J. Gibson, A. C. Peacock, and Z. Liu, "All-fibre heterogeneously-integrated frequency comb generation using silicon core fibre," Nat. Commun. **13**, 3992 (2022).

[9] S. Song, N. Healy, S. Svendsen, U. Österberg, A. V. C. Covian, J. Liu, A. Peacock, J. Ballato, F. Laurell, M. Fokine, and U. J. Gibson, "Crystalline GaSb-core optical fibers with room-temperature photoluminescence," Opt. Mater. Express **8**, 1435–1440 (2018).

[10] S. Song, K. Lønsethagen, F. Laurell, T. Hawkins, J. Ballato, M. Fokine, and U. J. Gibson, "Laser restructuring and photoluminescence of glass-clad GaSb/Si-core optical fibres," Nat. Commun. **10**, 1790 (2019).

[11] J. Zhang, T. Zhang, H. Zhang, Z. Wang, C. Li, Z. Wang, K. Li, X. Huang, M. Chen, Z. Chen *et al.*, "Single-crystal SnSe thermoelectric fibers via laser-induced directional crystallization: From 1D fibers to multidimensional fabrics," Adv. Mater. **32**, 2002702 (2020).

[12] D. A. Coucheron, M. Fokine, N. Patil, D. W. Breiby, O. T. Buset, N. Healy, A. C. Peacock, T. Hawkins, M. Jones, J. Ballato, and U. J. Gibson, "Laser recrystallization and inscription of compositional microstructures in crystalline SiGe-core fibres," Nat. Commun. **7**, 13265 (2016).

[13] J. R. Sparks, R. He, N. Healy, M. Krishnamurthi, A. C. Peacock, P. J. Sazio, V. Gopalan, and J. V. Badding, "Zinc selenide optical fibers," Adv. Mater. **23**, 1647–1651 (2011).

[14] T. Zaengle, U. J. Gibson, T. W. Hawkins, C. McMillen, B. Ghimire, A. M. Rao, and J. Ballato, "A novel route to fibers with incongruent and volatile crystalline semiconductor cores: GaAs," ACS Photonics **9**, 1058–1064 (2022).

[15] A. Peacock, U. Gibson, and J. Ballato, "Silicon optical fibres—Past, present, and future," Adv. Phys.: X **1**, 114–127 (2016).

[16] N. Healy, U. Gibson, and A. C. Peacock, "A review of materials engineering in silicon-based optical fibres," Semicond. Sci. Technol. **33**, 023001 (2018).

[17] M. G. Coco, S. C. Aro, S. A. McDaniel, A. Hendrickson, J. P. Krug, P. J. Sazio, G. Cook, V. Gopalan, and J. V. Badding, "Continuous wave Fe^{2+}:ZnSe mid-IR optical fiber lasers," Opt. Express **28**, 30263–30274 (2020).

[18] F. Deng, Y. Ren, Z. Wang, S. Xia, Z. Gu, and Y. Wang, "Microfibers doped with perovskite nanocrystals for ultralow-loss waveguides," ACS Appl. Nano Mater. **2**, 6585–6591 (2019).

[19] Z. Wang, H. He, S. Liu, H. Wang, Q. Zeng, Z. Liu, Q. Xiong, and H. J. Fan, "Air stable organic–inorganic perovskite nanocrystals@polymer nanofibers and waveguide lasing," Small **16**, 2004409 (2020).

[20] W. Wang, M. Zhang, F. Deng, Z. Wang, and Y. Wang, "Hybrids of perovskite nanocrystals and SiO_2 microfiber for robust and long-haul transmittable fiber lasers," Appl. Phys. Lett. **119**, 051102 (2021).

[21] N. Kurahashi, V.-C. Nguyen, F. Sasaki, and H. Yanagi, "Whispering gallery mode lasing in lead halide perovskite crystals grown in microcapillary," Appl. Phys. Lett. **113**, 011107 (2018).

[22] Y. Zhou, M. A. Parkes, J. Zhang, Y. Wang, M. Ruddlesden, H. H. Fielding, and L. Su, "Single-crystal organometallic perovskite optical fibers," Sci. Adv. **8**, eabq8629 (2022).

[23] R. Zhang, J. Fan, X. Zhang, H. Yu, H. Zhang, Y. Mai, T. Xu, J. Wang, and H. J. Snaith, "Nonlinear optical response of organic–inorganic halide perovskites," ACS Photonics **3**, 371–377 (2016).

[24] M. R. Filip, G. E. Eperon, H. J. Snaith, and F. Giustino, "Steric engineering of metal-halide perovskites with tunable optical band gaps," Nat. Commun. **5**, 5757 (2014).

[25] F. O. Saouma, D. Y. Park, S. H. Kim, M. S. Jeong, and J. I. Jang, "Multiphoton absorption coefficients of organic–inorganic lead halide perovskites $CH_3NH_3PbX_3$ (X = Cl, Br, I) single crystals," Chem. Mater. **29**, 6876–6882 (2017).

[26] H. Syed, W. Kong, V. Mottamchetty, K. J. Lee, W. Yu, V. R. Soma, J. Yang, and C. Guo, "Giant nonlinear optical response in triple cation halide mixed perovskite films," Adv. Opt. Mater. **8**, 1901766 (2020).

[27] G. Walters, B. R. Sutherland, S. Hoogland, D. Shi, R. Comin, D. P. Sellan, O. M. Bakr, and E. H. Sargent, "Two-photon absorption in organometallic bromide perovskites," ACS Nano **9**, 9340–9346 (2015).

[28] Y.-H. Kim, S. Kim, A. Kakekhani, J. Park, J. Park, Y.-H. Lee, H. Xu, S. Nagane, R. B. Wexler, D.-H. Kim *et al.*, "Comprehensive defect suppression in perovskite nanocrystals for high-efficiency light-emitting diodes," Nat. Photonics **15**, 148–155 (2021).

[29] R. J. Sutton, G. E. Eperon, L. Miranda, E. S. Parrott, B. A. Kamino, J. B. Patel, M. T. Hörantner, M. B. Johnston, A. A. Haghighirad, D. T. Moore, and H. J. Snaith, "Bandgap-tunable cesium lead halide perovskites with high thermal stability for efficient solar cells," Adv. Energy Mater. **6**, 1502458 (2016).

[30] W. Shen, J. Chen, J. Wu, X. Li, and H. Zeng, "Nonlinear optics in lead halide perovskites: Mechanisms and applications," ACS Photonics **8**, 113–124 (2020).

[31] Z.-K. Tan, R. S. Moghaddam, M. L. Lai, P. Docampo, R. Higler, F. Deschler, M. Price, A. Sadhanala, L. M. Pazos, D. Credgington *et al.*, "Bright light-emitting diodes based on organometal halide perovskite," Nat. Nanotechnol. **9**, 687–692 (2014).

[32] C. Li, H. Wang, F. Wang, T. Li, M. Xu, H. Wang, Z. Wang, X. Zhan, W. Hu, and L. Shen, "Ultrafast and broadband photodetectors based on a perovskite/organic bulk heterojunction for large-dynamic-range imaging," Light: Sci. Appl. **9**, 31 (2020).

[33] B. R. Sutherland and E. H. Sargent, "Perovskite photonic sources," Nat. Photonics **10**, 295–302 (2016).

[34]H.-Y. Ye, Y.-Y. Tang, P.-F. Li, W.-Q. Liao, J.-X. Gao, X.-N. Hua, H. Cai, P.-P. Shi, Y.-M. You, and R.-G. Xiong, "Metal-free three-dimensional perovskite ferroelectrics," Science **361**, 151–155 (2018).
[35]M. G. Ehrenreich, Z. Zeng, S. Burger, M. R. Warren, M. W. Gaultois, J.-C. Tan, and G. Kieslich, "Mechanical properties of the ferroelectric metal-free perovskite [MDABCO](NH_4)I_3," Chem. Commun. **55**, 3911–3914 (2019).
[36]D. Sirbu, H. C. L. Tsui, N. Alsaif, S. Iglesias-Porras, Y. Zhang, M. Wang, M. Liu, A. C. Peacock, P. Docampo, and N. Healy, "Wide-band-gap metal-free perovskite for third-order nonlinear optics," ACS Photonics **8**, 2450–2458 (2021).
[37]T. W. Kasel, Z. Deng, A. M. Mroz, C. H. Hendon, K. T. Butler, and P. Canepa, "Metal-free perovskites for non linear optical materials," Chem. Sci. **10**, 8187–8194 (2019).
[38]T. Handa, R. Hashimoto, G. Yumoto, T. Nakamura, A. Wakamiya, and Y. Kanemitsu, "Metal-free ferroelectric halide perovskite exhibits visible photoluminescence correlated with local ferroelectricity," Sci. Adv. **8**, eabo1621 (2022).
[39]X. Song, Q. Li, J. Han, C. Ma, Z. Xu, H. Li, P. Wang, Z. Yang, Q. Cui, L. Gao *et al.*, "Highly luminescent metal-free perovskite single crystal for biocompatible x-ray detector to attain highest sensitivity," Adv. Mater. **33**, 2102190 (2021).
[40]N. Gupta, C. McMillen, R. Singh, R. Podila, A. Rao, T. Hawkins, P. Foy, S. Morris, R. Rice, K. Poole *et al.*, "Annealing of silicon optical fibers," J. Appl. Phys. **110**, 093107 (2011).
[41]D. Marcuse, "Loss analysis of single-mode fiber splices," Bell Syst. Tech. J. **56**, 703–718 (1977).
[42]T. Ehmke, A. Knebl, S. Reiss, I. R. Fischinger, T. G. Seiler, O. Stachs, and A. Heisterkamp, "Spectral behavior of second harmonic signals from organic and non-organic materials in multiphoton microscopy," AIP Adv. **5**, 084903 (2015).
[43]Y. Gao, S. Meshkat, A. Johnston, C. Zheng, G. Walters, Q. Feng, X. Wang, M.-J. Sun, A. M. Najarian, D. Xue *et al.*, "Electro-optic modulation using metal-free perovskites," ACS Appl. Mater. Interfaces **13**, 19042–19047 (2021).
[44]X. Wang and Y. Yan, "Molecular engineering of metal-free perovskite MDABCO-NH_4I_3 towards enhanced ferroelectric polarization," arXiv:2206.11137 (2022).
[45]A. Vasilev, T. Deligeorgiev, N. Gadjev, and K.-H. Drexhage, "Synthesis of novel monomeric and homodimeric cyanine dyes based on oxazolo[4,5-b]pyridinium and quinolinium end groups for nucleic acid detection," Dyes Pigm. **66**, 135–142 (2005).
[46]A. Kurutos, I. Orehovec, D. Saftić, L. Horvat, I. Crnolatac, I. Piantanida, and T. Deligeorgiev, "Cell penetrating, mitochondria targeting multiply charged DABCO-cyanine dyes," Dyes Pigm. **158**, 517–525 (2018).